JOURNAL OF MATERIALS SCIENCE **39** (2004) 6191–6201

Synthesis of cobalt-aluminum spinels via EDTA chelating precursors

CUIYAN WANG, XUAN BAI
AnShan Normal University, Anshan 114005, People's Republic of China

SHAOMIN LIU
Institute of Environmental Science and Engineering, Nanyang Technological University, 18 Nanyang Drive, Singapore 637723

LIHONG LIU*
Institute of Bioengineering and Nanotechnology, 51 Science Park Road, Singapore Science Park II, Singapore 117586
E-mail: lhliu@ibn.a-star.edu.sg

In this work, synthesis of nanocrystalline $Co^{II}Co^{III}_xAl_{2-x}O_4$ (where $x = 0$, 0.5, 0.8, 1, 1.18 and 2) spinels by the thermal decomposition of complex precursors derived from metal nitrate salts and ethylenediaminetetraacetic acid (EDTA) has been systematically studied. Based on XRD, FTIR, DTA, TGA, SEM and TEM analyses, it has been found that the as-prepared metal organic precursors with different Co and Al contents display different thermal behavior, crystal development and particle morphology. Increment of Co content in precursors improves the degree of crystallinity of the powder. Treated at 400°C, in contrast to the well formed Co_3O_4 or Co_3O_4-like spinel structure for the powder precursors containing higher Co content, most of the powders from precursors containing lower Co content are still amorphous. Higher Co content in the precursors slightly decreases the unit cell parameters of the resulting $Co^{II}Co^{III}_xAl_{2-x}O_4$ spinels. Prepared at 900°C, the unit cell parameters of $Co^{II}Al_2O_4$, $Co^{II}Co^{III}_{0.5}Al_{1.5}O_4$, $Co^{II}Co^{III}AlO_4$, $Co^{II}Co^{III}_2O_4$ are 8.1038, 8.1007, 8.0867, and 8.0834 Å, respectively. Based on this work, preparation of a series of the $Co^{II}Co^{III}_xAl_{2-x}O_4$ spinels including black or bright blue $Co^{II}Al_2O_4$, $Co^{II}Co^{III}_{0.5}Al_{1.5}O_4$, $Co^{II}Co^{III}AlO_4$, $Co^{II}Co^{III}_2O_4$ from EDTA-Co(Al) complexing precursor has been established.

1. Introduction

Homogeneous and highly crystalline nano-phased composite powders have been widely studied for their potential in electrochemical [1–3], magnetic [4], catalytic [5, 6] and ceramic [7] applications. One example that has received particular attention in the literature is the cobalt-aluminate material system from which $Co^{II}Co^{III}_xAl_{2-x}O_4$ spinels (where $x = 0$ to 2) can be obtained [7–11]. Usually, powder composite materials are produced by conventional solid-state reactions [12]. Such fabrication methods often lead to two disadvantages: (i) the milling and grinding, normally employed to obtain a mixture (Co and Al oxides), can hardly obtain a micro-homogeneous phase structure and introduces contaminates, which have a detrimental effect on the material properties; and (ii) the mechanically-ground mixture requires prolonged calcination at high temperatures (>1400°C), which often promotes the undesirable crystallite growth. Therefore, conventional standard method of mechanically mixing two or several compounds followed by calcining and ball milling is not adequate for many advanced applications. It is necessary to develop new method to fabricate these nano-phased powders.

In order to obtain homogeneous fine powders, various solution-route preparation methods have been extensively investigated, such as sol-gel [13], co-precipitation [14], hydrothermal [15], and thermal decomposition of organic precursors [16]. Among these techniques, the thermal treatment of metal organic precursors, which are based on water-soluble complex methods to obtain the homogeneity of the metal ion distribution on the atomic level, is currently attracting considerable attention in the synthesis of complex materials, due to its safe, simple and fast features. The basic idea of this chelating complex process is to reduce the segregation of different metal ions during precipitation by forming stable metal-chelating complexes, since most common solutions containing two types of metal ions would on evaporation form a mixture of crystals of varying sizes and composition depending upon the ions present, solvent, rate of

*Author to whom all correspondence should be addressed.

evaporation, and so on. Ignition of the xerogel intermediates, at a relatively low temperature, removes the organic material and leaves the selected compositions of mixed oxides, chemically combined, pure, uniform, and in a molecular-scale finely divided state.

In this research work, the complex materials of $Co^{II}Co^{III}_xAl_{2-x}O_4$ (where $x = 0$ to 2) crystalline spinels derived from Co-Al-EDTA complexes were systematically investigated. EDTA possesses strong complexing ability for almost all metal-ions, and therefore, it was chosen as the complexing agent. It prevents partial segregation of metal compounds, which would occur in the case when ligands with discriminating complexing property to metal ions were used. In view of its simplicity and many unique features, we expect that the present method would be useful for providing an alternative of low cost mass productions of Co_3O_4 spinel, blue $CoAl_2O_4$ ceramic pigment, and other $Co^{II}Co^{III}_xAl_{2-x}O_4$ nanoderivatives.

2. Experimental

2.1. Chemicals

$Co(NO_3)_2{\cdot}6H_2O$ (>98%, Fluka), $Al(NO_3)_3{\cdot}9H_2O$ (>98.5%, Merck), Ethylenediaminetetraacetic acid (EDTA, >99.999%, Aldrich), and $NH_3{\cdot}H_2O$ (30–33%, Merck) were used as received.

2.2. Synthesis of the chelating precursors

A representative procedure of Co-Al-EDTA precursors is as follows: EDTA powder was introduced with magnetic stirring into 36 ml distilled water placed in a 400 ml beaker. Aqueous ammonia was then added dropwise to the beaker to facilitate the dissolution of EDTA, which converted EDTA into a water-soluble ammonium salt. The resulting solution had a pH of 8 to 10. After that, the required stoichiometric amounts of $Al(NO_3)_3{\cdot}9H_2O$ and $Co(NO_3)_2{\cdot}6H_2O$ were introduced with magnetic stirring into the above prepared EDTA ammonium solution. Six $Co^{II}Co^{III}_xAl_{2-x}O_4$ precursors with different Co/Al molar ratios were investigated and their compositions of the feedstock are given in Table I. The whole mixture (45 ml) containing metal ion and EDTA complexes was then stirred at 80°C for several hours until the solution became completely transparent with a purple colour. The purple solution was further heated at 90°C overnight to remove excess water and promote polymerization. During continued heating, the solution became more viscous and finally turned into a xerogel. The exposure of xerogel to atmosphere would lead to absorption of water and therefore the powder precursors should be preserved under moisture proof condition.

2.3. Preparation of $Co^{II}Co^{III}_xAl_{2-x}O_4$ spinels via pyrolysis

The resulting highly viscous solids or xerogels were pyrolyzed and calcined (in a carbolite furnace) under an airflow of 50 ml/min to a desired temperature at a heating rate of 2°C/min. The temperature was maintained for 2 h to remove the carbon residues. The cooling was carried out to room temperature at a cooling rate of 2°C/min. The final product samples–black or blue powders were taken for further material characterisation.

2.4. Characterization techniques

2.4.1. Thermal analysis

Thermogravimetric analysis (TGA) was carried out by TA instrument (TGA 2050). 5 mg precursor was placed in sample holder and heated from 25 to 600 °C at a rate of 5°C/min in air or nitrogen (flow rate = 90 ml/min), while weight change was recorded as a function of temperature. Differential thermal analyses (DTA) were performed in a Perkin-Elmer DTA instrument. 5 mg of sample was used and heated from 25 to 600°C at a rate of 2°C/min in air or nitrogen (flow rate = 50 ml/min), while heat flux changes were also recorded as a function of temperature.

2.4.2. FTIR investigation

The Fourier transform infrared (FTIR) spectra of the dried gels/chelating precursors or sintered powders at different conditions were obtained on a Shimadzu FTIR-8101 by employing potassium bromide (KBr) pellet technique.

2.4.3. XRD measurement

Structural phases were determined for sintered powders in a Shimadzu X-ray diffractometer using Cu K_a radiation. A continuous scan mode was used to collect 2θ data from 10° to 80° with a 0.02 sampling pitch and a 2°/min scan rate. X-ray tube voltage and current were set at 40 kV and 30 mA respectively.

TABLE I The feedstock of the synthesized EDTA-Co(Al) complexes

Sample name	Co/Al (Molar ratio)	$Co(NO_3)_2{\cdot}6H_2O$ (m mol)	$Al(NO_3)_3{\cdot}9H_2O$ (m mol)	EDTA (m mol)	$NH_3{\cdot}H_2O$ (m mol)
Pr-1	0.50	3.75	7.5	11.25	45
Pr-2	1.00	7.50	7.5	15.00	60
Pr-3	1.50	11.25	7.5	18.75	75
Pr-4	2.00	15.00	7.5	22.50	90
Pr-5	2.64	19.80	7.5	22.50	90
Pr-6	$+\infty$	7.50	0.0	7.50	30

Precursor: metal ion(s)—organic complex before pyrolysis.

2.4.4. SEM measurement

Morphologies of the sintered powders were observed using a scanning electron microscope (model Jeol JSM-5600LV).

2.4.5. TEM investigation

Structures of spinel particles was also investigated by transmission electron microscopy (model Philips CM300 FEG) at 300 kV accelerating voltage. A copper grid coated with carbon and formava film was used to disperse the powder that has been mixed with acetone and treated in ultrasonic bath.

3. Results and discussions

3.1. Formation of chelating precursors

Ethylenediaminetetraacetic acid (EDTA) is a well-known chelating agent with six potential sites (four carboxyl and two amino groups) for binding with metal cations. EDTA has a simplified formula, H_4Y, and usually forms 1:1 (molar ratio) complexes with most metal ions regardless of the charge of the cations. In this research work, the used EDTA compound in chelating reactions is the ammonia salt, $(NH_4)_4Y$ (or Y^{4-}). The complexation of Co^{2+}(Al^{3+}) and EDTA in solution follows the following two equations:

$$Co^{2+} + Y^{4-} \overset{K_1}{\longleftrightarrow} CoY^{2-} \quad (1)$$

$$Al^{3+} + Y^{4-} \overset{K_2}{\longleftrightarrow} AlY^{-} \quad (2)$$

The extent to which Co^{2+}(Al^{3+}) and EDTA complex formation occurs is usually expressed by the formation constant, K, for the above association reactions. According to the data reported in literature [17], $\log K_1$ and $\log K_2$ (at 20°C and ionic strength = 0.1) are 16.1 and 16.3, respectively. Under such conditions, all Al^{3+} and Co^2 were quantitatively converted to the complexes and no free metal ions were presented in the resulting co-ordination solution. Deep-purple transparent gel-like precursors were obtained when the aqueous solutions were thickened. Because no precipitation occurred over the entire concentration process, the compositional homogeneity of the two metal ions in the aqueous solution could be well maintained in the resulting gels. The characteristic IR absorption bands of pure EDTA and its metal complex precursors are classified in Table II. One can see that, with respect to one particular group, such as carboxylate, its characteristic IR absorption frequency varies within a certain range after coordination. The FT-IR spectra of the pure EDTA and Pr-2 are compared in Fig. 1. The C=O and C–O

TABLE II FTIR characteristic absorption of EDTA and chelating precursors

Sample name	IR (cm^{-1}) main bands
Pure EDTA	1043 ν_a (C–N); 1314 ν_s (C–O); 1694 ν_s (C=O)
Pr-1	1106 ν_a (C–N); 1398 ν_s (C–O); 1600 ν_s (C=O)
Pr-2	1106 ν_a (C–N); 1385 ν_s (C–O); 1600 ν_s (C=O)
Pr-3	1106 ν_a (C–N); 1400 ν_s (C–O); 1596 ν_s (C=O)
Pr-4	1106 ν_a (C–N); 1398 ν_s (C–O); 1602 ν_s (C=O)
Pr-5	1103 ν_a (C–N); 1399 ν_s (C–O); 1596 ν_s (C=O)
Pr-6	1106 ν_a (C–N); 1403 ν_s (C–O); 1593 ν_s (C=O)

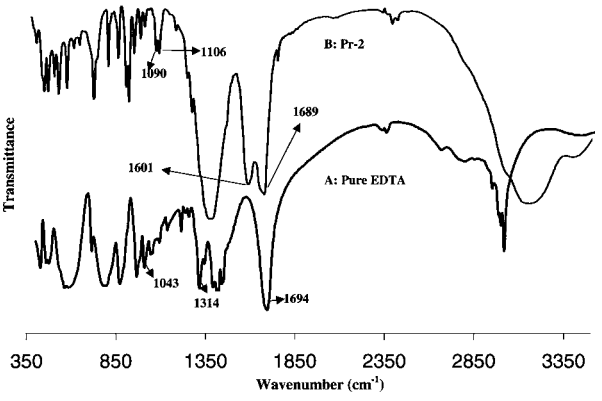

Figure 1 FTIR patterns of pure EDTA and Pr-2.

bonds stretching absorption in pure EDTA occurred as narrow bands, having a maximum absorption at 1694 cm^{-1} and a medium absorption at 1314 cm^{-1}, respectively (Fig. 1A) [18]. The coordinated C=O stretching absorption, on the other hand, appears at a relatively broad band, clearly consisting of two peaks at 1601 and 1689 cm^{-1} (Fig. 1B) [19]. The coordinated C–O bond stretching absorption again appears at a relatively broad band with the corresponding peaks at 1385 cm^{-1} (Fig. IB) [20]. The above changes in the stretching absorption band can be attributed to the absorption of four COO groups of the coordinated EDTA. The minor peak at 1043 cm^{-1} in Fig. 1A is attributable to the vibration of C–N bonds [21] in pure chelating ligand-EDTA. However, after coordination with metal ions, the C–N bond absorption band consists of two peaks at 1090 and 1106 cm^{-1}. This phenomenon may be due to the fact that the Co or Al atom of the complex anion is bonded octahedrally to the two nitrogen atoms.

3.2. Thermal evolution to $Co^{II}Co^{III}_xAl_{2-x}O_4$ spinel

The as-prepared EDTA-Co-Al gels are amorphous. The crystalline $Co^{II}Co^{III}_xAl_{2-x}O_4$ spinels were obtained by pyrolysis and calcination of these amorphous precursors at higher temperatures (from 250 to 1000°C) for 2 h. The development of spinel crystalline phase from precursors as a function of calcining temperature is explained by the analysis of XRD, TEM, FTIR, DTA/TGA, XPS and SEM results. In this work, all the crystalline phase development of the prepared 6 precursors is closely related to the $Co^{II}Co^{III}_xAl_{2-x}O_4$ spinel structure. Most of these precursors have the same thermal evolutional trend, particularly for these containing the same kinds of metal ions (i.e., Pr-1 to Pr-5). Therefore, emphasis is put only on two typical precursors (Pr-1 and Pr-6) to explain their crystal phase thermal evolution. A more detailed comparison of the crystalline phase development behaviour from the different precursors will be discussed in next section.

3.2.1. Thermal evolution to $Co^{II}Co^{III}Al_2O_4$ from Pr-1

The $Co^{II}Al_2O_4$ crystallite development from Pr-1 (where Co/Al = 0.5) as a function of calcining temperature is illustrated by the XRD patterns plotted in Fig. 2I.

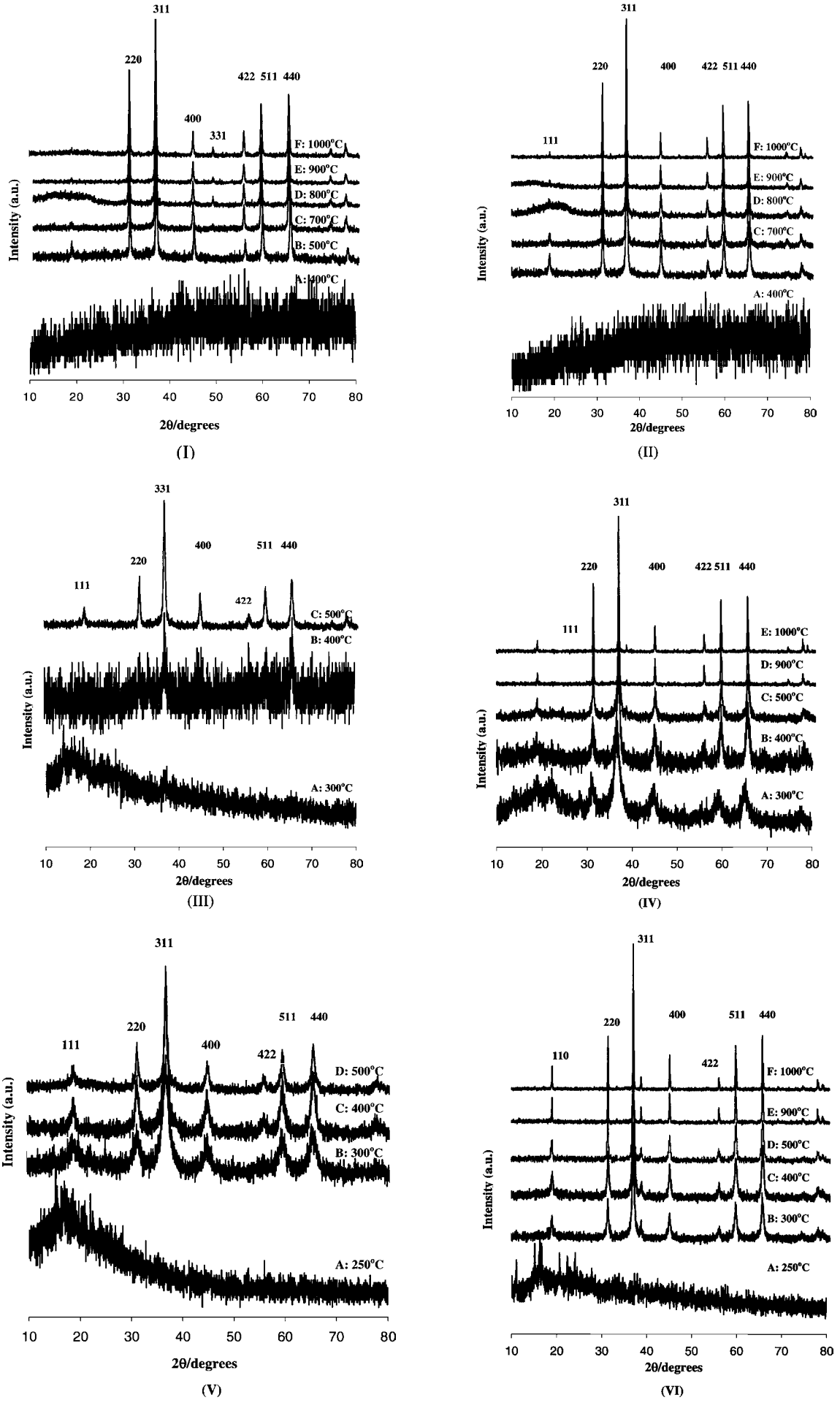

Figure 2 XRD patterns of spinel powders from different precursors calcined in air atmosphere for 2 h at various temperatures (I: Pr-1; II: Pr-2; III: Pr-3; IV: Pr-4; V: Pr-5; VI: Pr-6.

It is clear that most of the resultant powder at 400°C is still in amorphous state. At 500°C, the $CoAl_2O_4$ phases have been formed well, with all characteristic diffraction peaks of the cubic spinel phase. At higher temperature, the spinel phase patterns become more intense and the diffraction peaks reduce their widths gradually. An analysis based on the fwhm of (311) peaks indicates that the average size of spinel cystallites increases from 26 nm at 500°C to 28 nm at 700°C and the calculated lattice constant is ranged from 8.0966 to 8.1028 Å. Average crystallite sizes and lattice constant derived from other studied samples are also listed in Table III for a further comparison. When Pr-1 was sintered at a temperature higher than 700°C, for example, 800 and 900°C (D and E in Fig. 2I), the color of powder changed from black to bright blue. A new peak line at $2\theta = 49^\circ$ (lattice plane of {331}) is observed in the XRD patterns (E and F in Fig. 2I). The particle size is also increased from 28 nm (at 700°C) to 32 nm (at 900°C). The calculated lattice constant a_o (as shown in Table III) of the spinel cubic structure derived at 800 to 1000°C is very close to standard value of 8.104 Å for $CoAl_2O_4$ (JCPDS 44-0160), particularly for the powder thermally treated at 800°C for 8 h. In the studies of ceramic pigment $CoAl_2O_4$, some researchers [22] remarked that the only crystal phases of D, E and F in Fig. 2I where XRD patterns have the diffraction plane of {331} is the true $CoAl_2O_4$ phase whereas the former black powders obtained at lower temperatures (B and C in Fig. 2I) are the Co_3O_4-like intermediate phase. To be consistent with the definition of the majority of previous works [23, 24], we attribute all these phases (B, C, D, E, and F) to the $CoAl_2O_4$ structure. XRD patterns for other samples are also listed in Fig. 2 for a further analysis and comparison.

In agreement with the XRD results, the FTIR spectra shown in Fig. 3I also indicates an almost similar structural evolution from the Pr-1 samples. As can be seen from Fig. 3I, fingerprint IR absorption at 565 and 668 cm^{-1} for the $Co^{II}Al_2O_4$ spinel phase [25, 26] starts to appear at 400°C and develops fully at 500°C. When the calcination temperature increases to a temperature higher than 700°C, another band at around 500 cm^{-1} begins to appear. This indicates that the black $CoAl_2O_4$ phase and blue $CoAl_2O_4$ phase have different FTIR spectra. When the temperature is further increased to 900 or 1000°C, the band at 501 cm^{-1} appears with a higher intensity than that at 555 cm^{-1}, which was also observed by Zayat and Levy [22]. Three bands at 500, 555, and 662 to 650 cm^{-1} are attributed to the vibrational bands of blue $CoAl_2O_4$, which is a specific character on the FTIR absorption of $CoAl_2O_4$. From the effect of the calcination temperature on the IR absorptions of $CoAl_2O_4$, it indicated that blue phase $CoAl_2O_4$ can be formed at a temperature higher than 800°C, which agrees very well with the previous XRD studies. Figs 3II, 3III and 3IV display the FTIR spectrum thermal evolution of Pr-2, Pr-4 and Pr-6, respectively.

To have a better understanding on the above-described thermal processes, the TGA/DTA study for all the precursors was carried out during their pyrolysis in air environment. Table IV summarises some results

TABLE III The effect of calcination temperatures on the crystal structure of $Co^{II}Co_x^{III}Al_{2-x}O_4$ (where $x = 0$–2) spinels

Cal. Te. (°C)	XRD phases	Crystallite sizes (Å)	Lattic constant a_o (Å)
	Pr-1 (Co/Al = 0.5)		
400	Amorphous	~	~
500	$Co^{II}Al_2O_4$[b]	260.6	8.0966
600	$Co^{II}Al_2O_4$	275.2	8.0994
700	$Co^{II}Al_2O_4$	283.1	8.1028
800	$Co^{II}Al_2O_4$	306.2	8.1028
800 (8 h)	$Co^{II}Al_2O_4$	315.0	8.1040
900	$Co^{II}Al_2O_4$	326.1	8.1038
1000	$Co^{II}Al_2O_4$	351.5	8.1036
	Pr-2 (Co/Al = 1.0)		
400	Amorphous	~	~
500	$Co^{II}Co^{III}_{0.5}Al_{1.5}O_4$	209.3	8.0956
600	$Co^{II}Co^{III}_{0.5}Al_{1.5}O_4$	242.3	8.0972
700	$Co^{II}Co^{III}_{0.5}Al_{1.5}O_4$	243.4	8.0978
800	$Co^{II}Co^{III}_{0.5}Al_{1.5}O_4$	252.3	8.0986
900	$Co^{II}Co^{III}_{0.5}Al_{1.5}O_4$	374.1	8.1007
1000	$Co^{II}Co^{III}_{0.5}Al_{1.5}O_4$	571.7	8.1007
	Pr-3 (Co/Al = 1.5)		
300	Amorphous	~	~
400	Amorphous	~	~
500	$Co^{II}Co^{III}_{0.8}Al_{1.2}O_4$	191.4	8.0886
600	$Co^{II}Co^{III}_{0.8}Al_{1.2}O_4$	186.4	8.0903
	Pr-4 (Co/Al = 2.0)		
250	Amorphous	~	~
300	$Co^{II}Co^{III}AlO_4$	58.7	8.0776
400	$Co^{II}Co^{III}AlO_4$	119.8	8.1350
500	$Co^{II}Co^{III}AlO_4$	173.1	8.0839
600	$Co^{II}Co^{III}AlO_4$	174.2	8.0819
700	$Co^{II}Co^{III}AlO_4$	176.7	8.0850
800	$Co^{II}Co^{III}AlO_4$	447.9	8.0846
900	$Co^{II}Co^{III}AlO_4$	513.0	8.0867
1000	$Co^{II}Co^{III}AlO_4$	596.6	8.0855
	Pr-5 (Co/Al = 2.64)		
250	Amorphous	~	~
300	$Co^{II}Co^{III}_{1.18}Al_{0.82}O_4$	55.1	8.0816
400	$Co^{II}Co^{III}_{1.18}Al_{0.82}O_4$	98.5	8.0799
500	$Co^{II}Co^{III}_{1.18}Al_{0.82}O_4$	148.6	8.0804
600	$Co^{II}Co^{III}_{1.18}Al_{0.82}O_4$	255.3	8.0844
	Pr-6 (Co/Al =)		
250	Amorphous	~	~
300	$Co^{II}Co^{III}_2O_4$	179.9	8.0790
400	$Co^{II}Co^{III}_2O_4$	197.0	8.0836
500	$Co^{II}Co^{III}_2O_4$	239.4	8.0849
600	$Co^{II}Co^{III}_2O_4$	345.4	8.0844
700	$Co^{II}Co^{III}_2O_4$	462.3	8.0839
800	$Co^{II}Co^{III}_2O_4$	579.6	8.0833
900	$Co^{II}Co^{III}_2O_4$	581.3	8.0834
1000	$Co^{II}Co^{III}_2O_4$	623.7	8.0838

[a] As calculated data.
[b] All formulae in this column are apparent chemical formulae (311) peaks were used in these calculations for crystallite sizes of the spinel phase.

TABLE IV Main TGA characteristics of EDTA-Co-Al precursors

	Weight (%) change with the temperature in air			
Samples	150°C	300°C	400°C	500°C
Pr-1	96.80	51.13	12.70	9.50
Pr-2	96.17	53.05	13.32	12.99
Pr-3	97.99	56.91	13.47	13.26
Pr-4	97.30	60.70	15.19	15.17
Pr-5	97.93	52.67	15.22	15.12
Pr-6	87.10	51.10	12.80	12.60

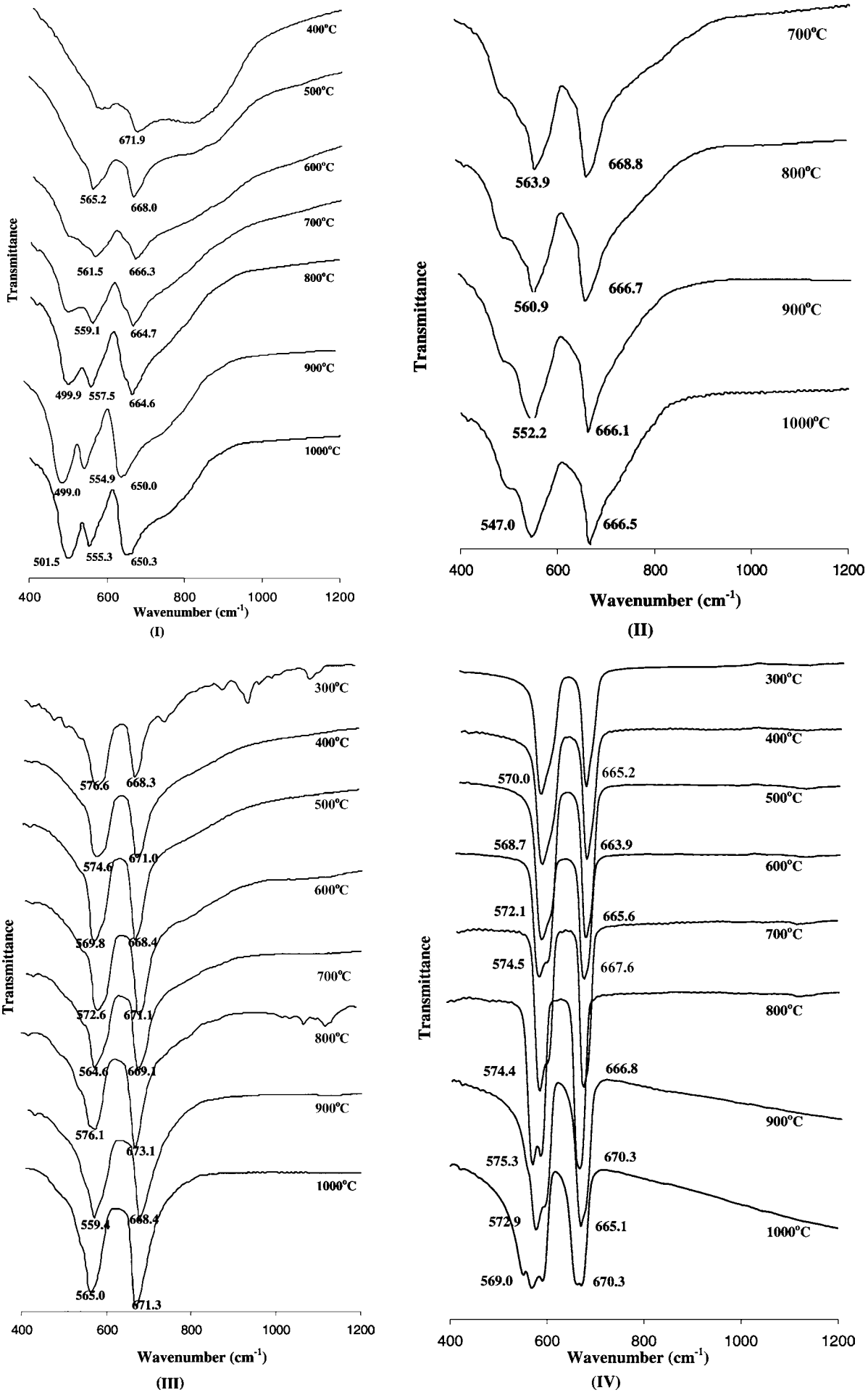

Figure 3 FTIR spectra of spinel powders from different precursors calcined in air atmosphere for 2 h at various temperatures (I: Pr-1; II: Pr-2; III: Pr-4; IV: Pr-6.

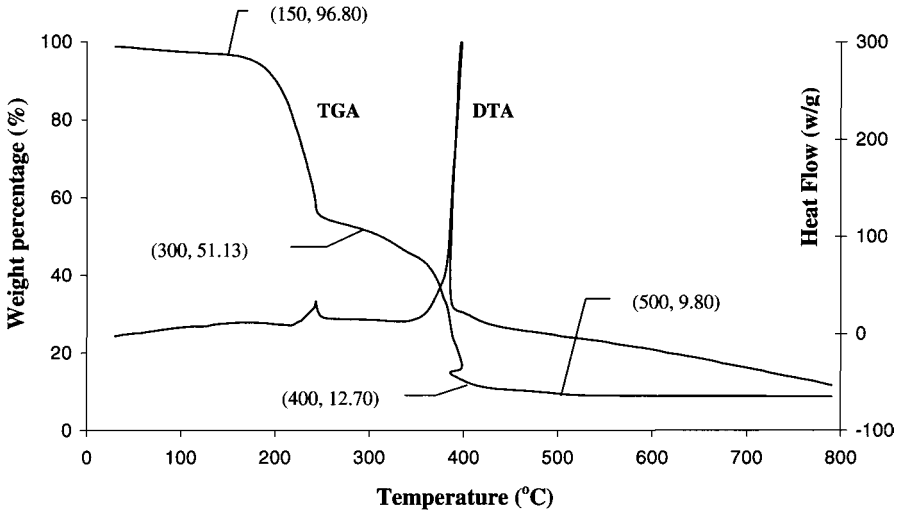

Figure 4 TGA and DTA profiles of Pr-1 in air atmosphere.

of TGA investigation. All the TGA curves show an obvious two-slope weight loss profile, with one between 150 and 300°C, and another one from 300 to 450°C. For example, the TGA/DTA profiles of Pr-1 are shown in Fig. 4. Before 150°C, the 3.2% weight loss is related to the dehydration of the precursor, since the intermediate xerogel is not dried completely and easily absorbs water. When the temperature is increased from 150 to 300°C, there is an obvious weight loss span of 45%. This is due to the decomposition of precursor. The second weight loss span of 40% occurs from 300 to 450°C. The difference between the two weight loss stages is that the burnout of organics takes place largely in the latter one, corresponding to the high exothermic peaks at 390°C in DTA curve (in Fig. 4). When the temperature is close to 400°C, the weight loss speed is very slow and the weight remains a constant regardless of further temperature increment.

The prepared $Co^{II}Co_x^{III}Al_{2-x}O_4$ spinel was also studied by HRTEM investigation. Fig. 5 shows the formation of $CoAl_2O_4$ at 1000°C from Pr-1. TEM image at low magnification (Fig. 5a) shows the particle agglomerates, from which small crystal particles with a size around 35 nm are clearly observed. This agrees with the crystallite size derived by XRD patterns in Table III. As the agglomerates consist of densely packed crystallites, it could not be easily dispersed. In addition to the clearly resolved {111} plane of $CoAl_2O_4$ (Fig. 5b), another fringe pattern with interplane distance as 2.8 ± 0.1 Å should be assigned to {220} plane of $CoAl_2O_4$ (Fig. 5c).

3.2.2. Thermal evolution of $Co^{II}Co_2^{III}O_4$ from Pr-6

Different from other precursors, Pr-6 contains only Co in the metal ion-EDTA complex. A set of XRD patterns for the powders prepared by pyrolysis and heat treatment at different temperatures are displayed in Fig. 2VI. Under oxidative atmosphere, the Co-EDTA gel readily decomposes at a temperature as low as 250°C. At only 300°C, the $Co^{II}Co_2^{III}O_4$ cubic spinel phase has been formed. Similar to samples prepared from Pr-1 gel, at higher temperatures, the spinel phase patterns become more intense and the diffraction peaks reduce their widths. As shown in Table III, the crystal size increases from 18 nm at 300°C to 62.4 nm at 1000°C and the calculated lattice constant is ranged from 8.079 to 8.084 Å. Fig. 6 is the HRTEM images of Pr-6 powder heated at 400°C. From Fig. 6a, it is clear that the prepared particle size is about 20 nm, which is in consistent with the calculated crystal size in Table III based on lattice plane of {331}. Examination of Fig. 6b clearly indicates inter-plane distance d_{111} of cubic $Co^{II}Co_2^{III}O_4$. Fig. 3IV is the FTIR spectra for the as-prepared Pr-6 samples. It is obvious that metal-oxygen vibrational absorption for the spinel phase can be fully developed at 300°C [27–29]. This agrees well with the XRD investigation.

Calcinating temperatures also show their effect on the surface morphology of the prepared spinel powder. The typical SEM images of the Pr-6, as well as their spinel powders obtained by calcination at different temperatures (i.e., 500 and 1000°C) are shown in Fig. 7. The size of the starting complex precursor can be estimated in the range of 10–160 μm. Each chunk having smooth surface will be decomposed into fine and porous grains after heat treatment. The particle agglomerate size of the resulting powders is very dependent on the temperature of heat treatment. Samples at 500°C are composed of very fine particles with the size ranged from 0.1 to 0.2 microns and the formed spinel particles are easily agglomerated to large sized particulates as shown in Fig. 7b. An increase in the heat treatment temperature promotes grain growth by a solid state reaction between the agglomerated particles. The driving force for such surface morphology change is the decrease of total surface energies, which comes about by grain contact and growth. For example, when the heat treatment temperature increases from 500 to 1000°C, inspection of Fig. 7c reveals that small spinel particles have grown into large micron sized particles and most of the particles are in the forms of uniform spheres with a size ranged from 0.5 to 1.5 μm.

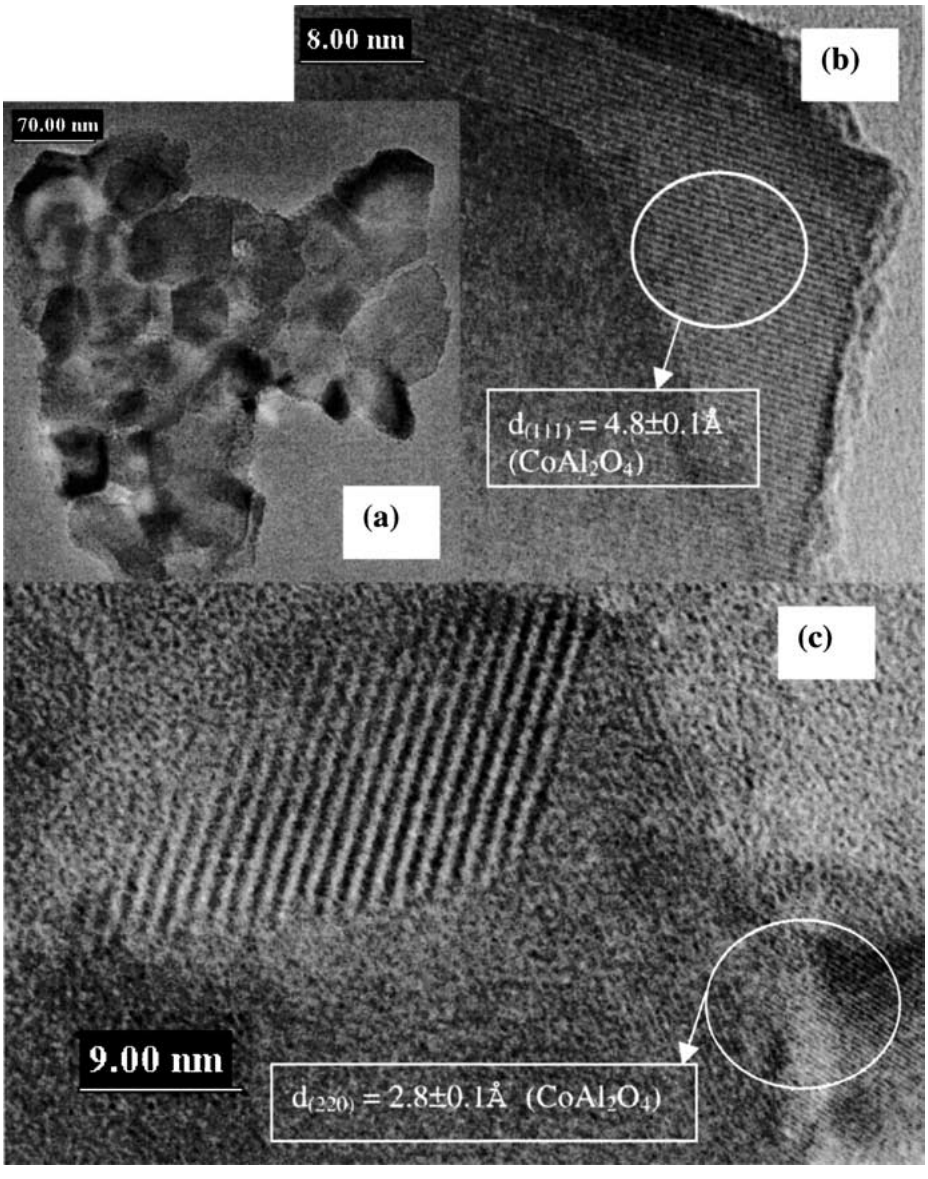

Figure 5 HRTEM images of spinel powder from Pr-1 calcined at 1000°C (b and c: an enlarged part of a).

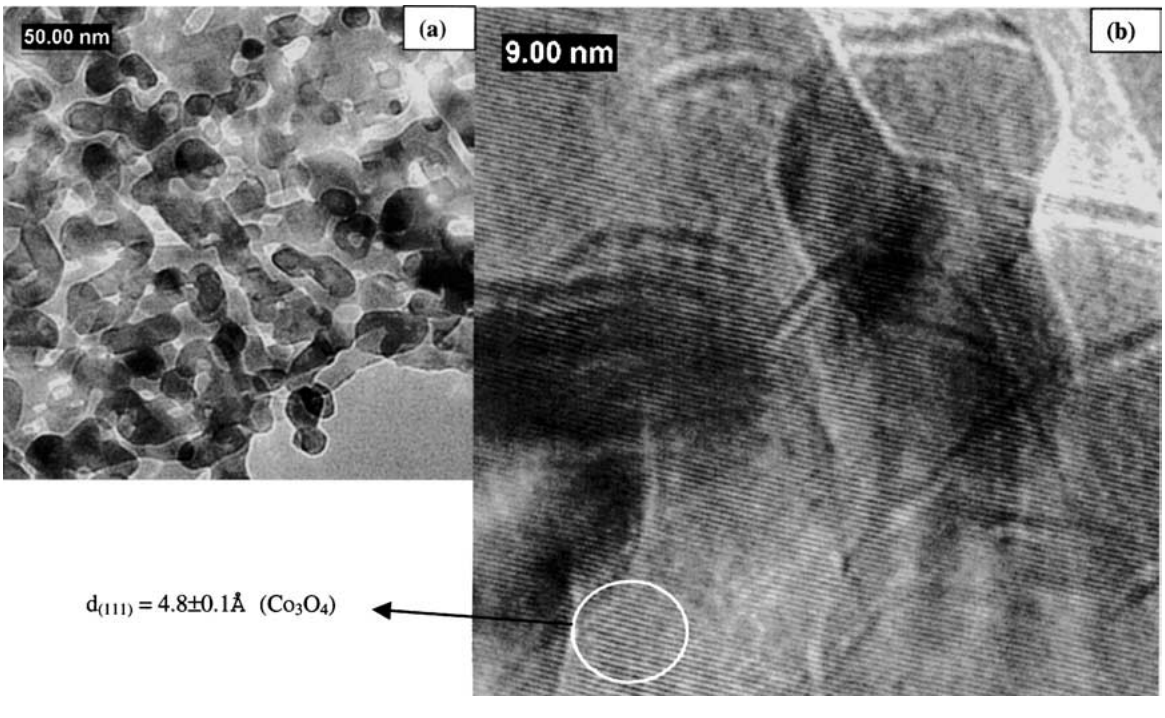

Figure 6 TEM images of spinel powder prepared from Pr-6 sintered at 400°C.

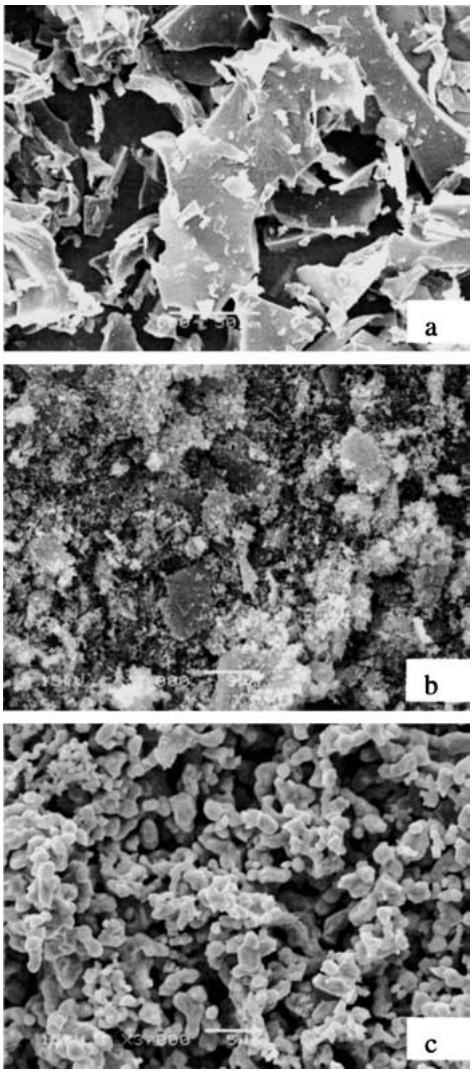

Figure 7 SEM images of Pr-6 and the prepared $Co^{II}Co^{III}O_4$ powders (a, precursor; b, c, $Co^{II}Co^{III}O_4$ prepared by pyrolysis/heat-treatment of Pr-6 at 500 and 1000°C, respectively).

3.3. Effects of Co content in the precursors on the development of $Co^{II}Co^{III}_xAl_{2-x}O_4$ spinels

In above sections, we described the $Co^{II}Co^{III}Al_2O_4$ and $Co^{II}Co^{III}_2O_4$ crystallite development from two different precursors calcined at various temperatures. Now, we will discuss the effect of Co contents in different precursors on the development of $Co^{II}Co^{III}_xAl_{2-x}O_4$ spinel. Spinel oxides belong to a class of complex oxides with the general formulas of AB_2O_4 in which A ions are divalent cations occupying tetrahedral sites and B ions are trivalent cations in octahedral sites. The cobalt aluminium oxide $CoAl_2O_4$ from Pr-1 belongs to this type of spinel. However, when the molar ratio of A to B is not in stoichiometry, inversion between A and B may be produced [30]. For example, when the molar ratio of A/B is greater than 0.5, not only B but also A cation (in case of the existence of two distinct ions A^{2+} and A^{3+}) will occupy the octahedral sites. This is the case of cobalt aluminium spinel oxide. Samples from Pr-1 to Pr-5 produced the crystals with chemical compositions of $Co^{II}Al_2O_4$, $Co^{II}Co^{III}_{0.5}Al_{1.5}O_4$, $Co^{II}Co^{III}_{0.8}Al_{1.2}O_4$, $Co^{II}Co^{III}AlO_4$ and $Co^{II}Co^{III}_{1.18}Al_{0.82}O_4$, respectively. Different from other precursors, there is no Al cation in Pr-6 (Co/Al = ∞) and its sintered sample shows the formation of crystal phase of $Co^{II}Co^{III}_2O_4$, among which the Co^{II} ($3d^7$) is in the tetrahedral sites and Co^{III} ($3d^6$) is in the octahedral sites.

XRD profiles of the above samples prepared from Pr-1 to Pr-6 are closely related to the Co_3O_4 like or Co_3O_4 spinel structure. All these compounds have the same spinel cubic (Fd3m) structure differing only slightly in the size of the lattice. A more detailed comparison of the XRD spectra (as shown in Fig. 2) will show the difference. Treated at 400°C, most of the powders from Pr-1 to Pr-3 are amorphous. However, at this same temperature, other precursors from Pr-4 to Pr-6 display Co_3O_4 or Co_3O_4-likespinel structure, with Pr-6 having the highest intensity. The relatively low temperature (300°C) at which the spinels can be largely formed is a distinguished characteristic for the precursors Pr-4 to Pr-6. This point can also be confirmed by checking the FTIR spectra of samples prepared from Pr-1 and Pr-6. Contrary to the weak metal-oxygen vibrational absorption from Pr-1 sample calcined at 400°C, the IR absorption for the spinel phase in Pr-6 sample is already fully developed at this temperature. All these indicate that increasing Co content in precursors improves the degree of crystallinity of the powder. Due to the different degree of crystallinity, the prepared $Co^{II}Co^{III}_xAl_{2-x}O_4$ spinels from different precursors show different powder morphology. Fig. 8a and b and Fig. 7c are the SEM images of $Co^{II}Al_2O_4$, $Co^{II}Co^{III}AlO_4$ and $Co^{II}Co^{III}_2O_4$, respectively. They were prepared at the same temperature of 1000°C from three different precursors (Pr-1, Pr-4, and Pr-6), but they display different powder morphology. In comparison with $Co^{II}Al_2O_4$ and $Co^{II}Co^{III}AlO_4$ which display large particle agglomerates in irregular shape, $Co^{II}Co^{III}_2O_4$ powder is in the form of uniform spherical particles. Although some $Co^{II}Co^{III}_2O_4$ particle aggregates still exist, these aggregates are weakly connected by a few particles. The increase of Co content in $Co^{II}Co^{III}_xAl_{2-x}O_4$ spinels slightly decreases the unit cell parameters. For example, prepared at 900°C, the unit cell parameters of $Co^{II}Al_2O_4$, $Co^{II}Co^{III}_{0.5}Al_{1.5}O_4$, $Co^{II}Co^{III}AlO_4$, $Co^{II}Co^{III}_2O_4$ are 8.1038, 8.1007, 8.0867, and 8.0834 Å, respectively.

As previously mentioned, bright blue $Co^{II}Al_2O_4$ can be obtained by calcination of Pr-1 at a temperature of 800°C (or above). However, no color change was observed in the spinel powders prepared from other precursors. The diffraction plane of {331} in the XRD pattern (as shown in Fig. 2I) and three vibrational bands at 500, 555, and 662 to 650 cm^{-1} in FTIR spectra (as shown in Fig. 3I) are attributed to the characteristics of blue $CoAl_2O_4$ phase. Examination of the XRD patterns and FTIR spectra of other samples in different temperatures, such phenomenon never occurs. For example, Fig. 2II and Fig. 3II are the XRD patterns and FTIR spectra, respectively, of spinel powders from Pr-2, where the cation ratio of Al^{3+} to Co^{2+} in starting metal solution is closest to that of Pr-1. At other similar preparing conditions, the diffraction plane of {331} and the band at around 500 cm^{-1} can not be observed from

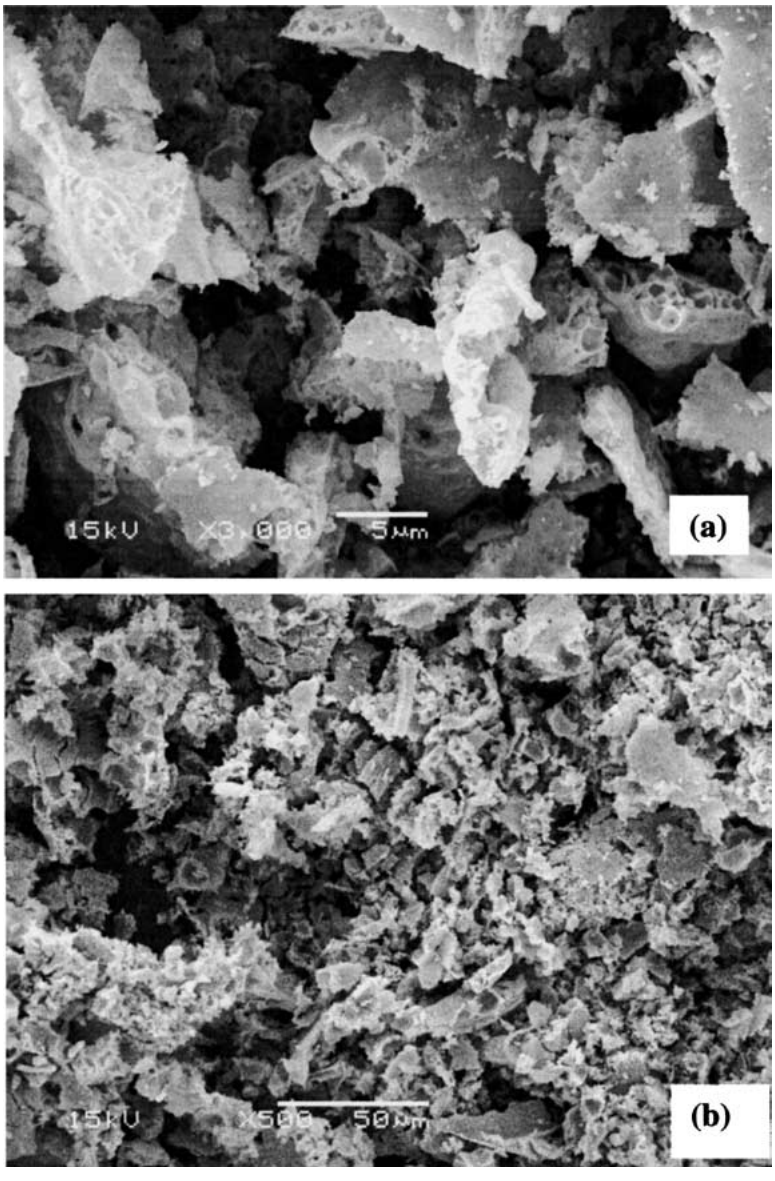

Figure 8 SEM images of $Co^{II}Co_x^{III}Al_{2-x}O_4$ powder calcined at 1000°C from different precursors (a: $Co^{II}Al_2O_4$ from Pr-1; b: $Co^{II}Co^{III}Al\,O_4$ from Pr-4).

its XRD and FTIR patterns. Compared to other black $Co^{II}Co_x^{III}Al_{2-x}O_4$ spinels, this bright blue $Co^{II}Al_2O_4$ has its unique characteristics of RXD pattern and FTIR spectra, which is strongly dependent on the temperature ($\geq$800°C) of heat treatment and the stoichiometry of Co and Al (Co/Al = 0.5) in the precursors. This gives us the information for fabrication of blue ceramic pigment. Compared to the conventional solid-state reaction method, the present research shows a substantial lowering of the processing time and temperature required for the formation of desired bright blue $Co^{II}Al_2O_4$ phase.

4. Conclusions

From the EDTA-Co-Al complexing precursors to the well-developed spinel crystals (by calcination of the starting precursors at different temperatures), the synthesis of $Co^{II}Al_2O_4$, $Co^{II}Co_{0.5}^{III}Al_{1.5}O_4$, $Co^{II}Co_{0.8}^{III}Al_{1.2}O_4$, $Co^{II}Co^{III}AlO_4$, $Co^{II}Co_{1.18}^{III}Al_{0.82}O_4$, and $Co^{II}Co_2^{III}O_4$ spinels has been investigated. The characterization techniques involve XRD, FTIR, DTA, TGA, XPS, SEM and HRTEM methods. Results indicate that the increment of Co content in precursors improves the degree of crystallinity of the powder. With the increase of Co content in $Co^{II}Co_x^{III}Al_{2-x}O_4$ spinels, the unit cell parameters slightly decrease. Based on this research work, preparation of a series of the $Co^{II}Co_x^{III}Al_{2-x}O_4$ spinels including $Co^{II}Al_2O_4$, $Co^{II}Co_{0.5}^{III}Al_{1.5}O_4$,$Co^{II}Co^{III}AlO_4$, $Co^{II}Co_2^{III}O_4$ from EDTA-Co(Al) complexing precursor has been well established.

Acknowledgements

The authors would like to express sincere gratitude to Professor Zeng Huachun for his insightful comments and valuable contributions towards the completion of this paper.

References

1. A. P. ALIVISATOS, *J. Phys. Chem.* **100** (1996) 13226.
2. K. OGURA, N. ENDO and M. NAKAYAMA, *J. Electrochem. Soc.* **145** (1998) 3801.
3. O. C. MONTEIRO, H. I. S. NOGUEIRA and T. TRINDADE, *Chem. Mater.* **13** (2001) 2103.

4. O. JARJAYES, P. H. FRIES and G. BIDAN, *Synth. Met.* **69** (1995) 343.
5. S. SWATHIRAJAN and Y. M. MIKHAIL, *J. Electrochem. Soc.* **39** (1992) 2105.
6. U. KANG, A. A. ZHILIN, G. T. PETROVSKY, O. S. DYMSHITS and T. I. CHUVAEVA, *J. Non-Cryst. Solids* **258** (1999) 216.
7. O. V. ANDRUSHKOVA, V. A. USHAKOV, V. A. POLUBOJAROV and E. G. AVVAKUMOV, *Sibirskii Khimicheskii Zhurnal* **3** (1992) 97.
8. E. ANTOLINI and E. ZHECHEVA, *Mater. Lett.* **35** (1998) 380.
9. M. E. BAYDI, G. POILLERAT, J. L. REHSPRINGER, J. L. GAUTIER, J. F. KOENIG and P. CHARTIER, *J. Solid State Chem.* **109** (1994) 281.
10. S. CHEMLAL, A. LARBOT, M. PERSIN, J. SARRAZIN, M. SGHYAR and M. RAFIQ, *Mater. Res. Bull.* **35** (2000) 2515.
11. W. S. CHO and M. KAKIHANA, *J. Alloy. Compd.* **287** (1999) 87.
12. S. J. SCHNEIDER, R. S. ROTH and J. L. WARING, *J. Res. NBS-A* **65A** (1961) 345.
13. L. JI, J. LIN, K. L. TAN and H. C. ZENG, *Chem. Mater.* **12** (2000) 931.
14. U. CHELLAM, Z. P. XU and H. C. ZENG, *Chem. Mater.* **12** (2000) 650.
15. E. L. UZUNOVA, I. G. MITOV and D. G. KLISSURSKI, *Bull. Chem. Soc. Jpn.* **70** (1997) 1985.
16. C. D. VEITCH, *J. Mater. Sci.* **26** (1991) 6527.
17. J. A. DEAN, "Lange's Handbook of Chemistry," 4th ed. (McGraw-Hill, New York, 1992).
18. L. HONG, F. GUO, and J. LIN, *Mater. Res. Bull.* **34** (1999) 1943.
19. K. NAKAMOTO, "Infrared and Raman Spectra of Inorganic and Coordination Compounds," 4th ed. (John Wiley, New York, 1986), p. 240
20. F. H. CHEN, H. S. KOO and T. Y. TSENG, *J. Amer. Ceram. Soc.* **75** (1992) 96.
21. C. J. POUCHERT (ed.), "The Aldrich Library of FT-IR Spectra," Aldrich Chemical Co., US, 1985.
22. M. ZAYAT and D. LEVY, *Chem. Mater.* **12** (2000) 2763.
23. S. CHOKKARAM, R. SRINIVASAN, D. R. MILBURN and B. H. DAVIS, *J. Mol. Catal. A: Chem* **121** (1997) 157.
24. F. ŠVEGL, B. OREL, P. BUKOVEC, K. KALCHER and M. G. HUTCHINS, *J. Electroanal. Chem.* **418** (1996) 53.
25. M. QIAN and H. C. ZENG, *J. Mater. Chem.* **7** (1997) 493.
26. L. JING, J. LIN and H. C. ZENG, *J. Phys. Chem.* B **104** (2000) 1783.
27. G. BUSCA, R. GUIDETTI and V. LORENZELLI, *J. Chem. Soc., Faraday Trans.* **96** (1990) 989.
28. R. A. NYQUIST and R. O. KAGEL, "The Handbook of Infrared and Raman Spectra of Inorganic Compounds and Organic Salts," Vol. 4, Infrared Sprectra of Inorganic Compounds (Academic Press Inc., 1997) p. 219.
29. F. F. BENTLEY, L. D. SMITHSON and A. L. ROZEK, "Infrared Spectra and Characteristic Frequencies 700–300 cm^{-1}" (Interscience, New York, 1968).
30. A. F. WELLS, "Structural Inorganic Chemistry," 5th ed. (Clarendon Press, Oxford, 1984) p. 594.

Received 4 November 2003
and accepted 28 May 2004